

All-Optical Digital Logic Based on Unidirectional Modes

Jie Xu,* Yamei Luo, Sanshui Xiao, Fengwen Kang,* and Kosmas L. Tsakmakidis*

Standard electronic computing based on nanoelectronics and logic gates has upended our lives in a profound way. However, suffering from, both, Moore's law and Joule's law, further development of logic devices based solely on electricity has gradually stuck in the mire. All-optical logic devices are believed to be a potential solution for such a problem. This work proposes an all-optical digital logical system (AODLS) based on unidirectional (one-way propagation) modes in the microwave regime. In a Y-shaped module of the AODLS, the basic seven logic gates, including OR, AND, NOT, NOR, NAND, XOR, and XNOR gates, are achieved for continuous broadband operation relying on the existence of unidirectional electromagnetic signals. Extremely large extinction and contrast ratios are found in these logic gates. The idea of "negative logic" is used in designing the AODLS. Moreover, the authors further demonstrate that the AODLS can be assembled to multi-input and/or multi-output logical functionalities, which is promising for parallel computation. Besides, numerical simulations perfectly fit with and corroborate the theoretical analyses presented here. The low-loss, broadband, and robust characteristics of this system are outlined and studied in some detail. The AODLS consisting of unidirectional structures may open a new route for all-optical calculation and integrated optical circuits.

1. Introduction


Moore's law has indicated and underlined the direction for the development of electrical communication for almost 50 years now. To achieve even faster communications with less energy consumption and smaller devices, a new generation of devices is needed. Optical communication, owing to its ultra-fast data transmission, immune to cross-talk^[1,2] and minimal or even zero^[3] energy loss, is believed to be a promising candidate.

At present, many kinds of optical logic gates (LGs), have been achieved in micro-ring resonators,^[4–7] Mach–Zehnder interferometers,^[8–10] plasmonic nanostructures,^[11–14] photonic crystals (PhCs),^[15–18] microcavities,^[19,20] magnetic^[21,22] or 2D material-based systems.^[23–26] The aforementioned all-optical LGs are limited by one or more following conditions: 1) the discrete and/or narrow operating band,^[27] 2) different input–output frequencies ($f_{in} \neq f_{out}$),^[5,28] 3) the complex fabrication processes, and 4) relatively low signal-to-noise ratio. Besides, the logic states in the above LGs are dependent on the input–output energy intensities, or the polarizations/phase or DC potential, resulting in the low extinction ratio (ER) and contrast ratio (CR) between logic "0" and logic "1". To our knowledge, the ER and CR in the previously reported works are usually below 30 dB.^[29] To a certain extent, the values of the ER and CR could be enlarged by improving the manufacturing process or the monitoring technology. However, the

error rate (Er) will remain more or less the same. To achieve ultra-high-performance optical communication, precise logic states are required, and in this work, we shall show that the unidirectional mode-based devices have the potential for achieving this goal.

Unidirectional (one-way) modes are those electromagnetic (EM) modes that are allowed to propagate only in one direction. They can be attained in several different structures, for example, the magneto-optical (MO) heterostructures,^[30–34]

J. Xu, Y. Luo
School of Medical Information and Engineering
Southwest Medical University
Luzhou 646000, China
E-mail: xujie011451@163.com

 The ORCID identification number(s) for the author(s) of this article can be found under <https://doi.org/10.1002/adom.202201836>.

© 2022 The Authors. Advanced Optical Materials published by Wiley-VCH GmbH. This is an open access article under the terms of the Creative Commons Attribution License, which permits use, distribution and reproduction in any medium, provided the original work is properly cited.

^[†]Present address: College of Materials Science and Engineering, Sichuan University, Chengdu, 610065, China

DOI: 10.1002/adom.202201836

S. Xiao
DTU Fotonik
Department of Photonics Engineering
Technical University of Denmark
Kgs. Lyngby DK-2800, Denmark
F. Kang^[†]
Laboratory of Advanced Nano Materials and Devices
Institute of Materials Technology (IMT)
Ningbo Institute of Materials Technology and Engineering (NIMTE)
Chinese Academy of Sciences (CAS)
Ningbo 315201, China
E-mail: kangfengwen0597@126.com
K. L. Tsakmakidis
Section of Condensed Matter Physics
Department of Physics
National and Kapodistrian University of Athens
Panepistimioupolis, Athens GR-157 84, Greece
E-mail: ktsakmakidis@phys.uoa.gr

topological metamaterial,^[35] and topological photonic crystals (PhCs).^[36,37] The MO heterostructures, without doubt, are technically the most simple way to build one-way waveguides. The robust one-way propagating EM waves without backscattering have been observed in the laboratory by designing non-reciprocal MO PhCs.^[38] In 2017, we found that owing to the one-way property, the MO heterostructure terminated by metal layers could overcome the time-bandwidth limit because of the broken Lorentz reciprocity.^[31] Recently, we have proposed several MO one-way waveguides in which interesting functionalities such as slow light,^[30,39] bidirectionally rainbow trapping and releasing,^[40] and true rainbow trapping^[32,41] were achieved. The one-way propagation characteristic is very suitable and desired for designing LGs because the one-way modes are insensitive to disorders and bends,^[42,43] and the noise barely exists in such devices. However, how to assemble one-way structures flexibly and make them work as multiple LGs is currently an ongoing progress.^[44]

In this paper, we propose the LGs and the all-optical digital logical system (AODLS) based on robust unidirectional modes. In the AODLS, the ER and CR are found to diverge in theory, while the error rate (Er) is negligible. Applying the logical and negative logical concepts, multiple LGs are achieved in a single Y-shaped module of the AODLS for the whole relatively broad one-way band. More interestingly, besides the advantages of the enormous ER and CR and incredibly small Er, the

unidirectional-modes based AODLS could be used in parallel operation^[45] with multiple inputs and/or outputs due to its expandability. This work aims to point out a new path for all-optical calculations, with the simple universal AODLS being easily extendable to other higher regimes.

2. The Y-Shaped Module of the AODLS

In this subsection, we first study the propagation characteristics in the basic module of the AODLS. The schematic of the AODLS is shown in **Figure 1**. As one can see, the system is constructed by three basic elements/arms, that is, 'A', 'B', and 'C', which are built by three types of magnetized yttrium-iron-garnet (YIG) materials. The yellow and blue colored materials represent the YIG with remanence, and the magnetization directions are +z and -z, respectively. The last kind of the YIG layer is magnetized by an external magnetic field (EMF) B_0 (-z). For simplicity, the above YIG layers are named YIG-1, YIG-2, and YIG-3, respectively. The zoom-in picture in Figure 1 shows one of the basic Y-shaped modules of the AODLS. To clearly illustrate how the module works for logic operations, we investigate the propagation characteristics of the guiding modes in the arms 'A', 'B', and 'C'. Due to the existence of the magnetization, the relative permeability of YIG-1, YIG-2, and YIG-3, respectively takes the following forms

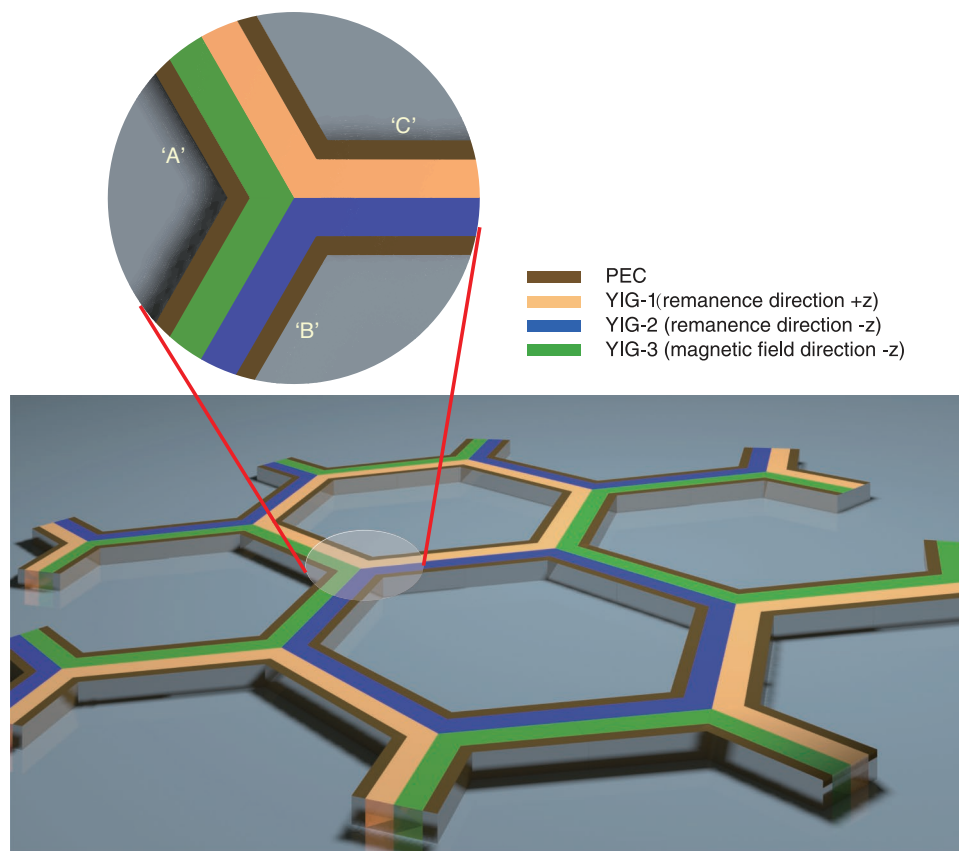


Figure 1. The schematic of the all-optical digital logical system (AODLS). The yellow, blue, and green colored materials represent YIG-1 with remanence (+z), YIG-2 with remanence (-z), and YIG-3 under an EMF (-z).

$$\begin{aligned} \bar{\mu}_{r1} &= \begin{bmatrix} \mu_{1r} & i\mu_{2r} & 0 \\ -i\mu_{2r} & \mu_{1r} & 0 \\ 0 & 0 & 1 \end{bmatrix} \\ \bar{\mu}_{r2} &= \begin{bmatrix} \mu_{1r} & -i\mu_{2r} & 0 \\ i\mu_{2r} & \mu_{1r} & 0 \\ 0 & 0 & 1 \end{bmatrix} \\ \bar{\mu} &= \begin{bmatrix} \mu_1 & -i\mu_2 & 0 \\ i\mu_2 & \mu_1 & 0 \\ 0 & 0 & 1 \end{bmatrix} \end{aligned} \quad (1)$$

where $\mu_{1r} = 1$, $\mu_{2r} = -\frac{\omega_r}{\omega}$, $\mu_1 = 1 + \frac{\omega_m \omega_0}{\omega_0^2 - \omega^2}$, and $\mu_2 = \frac{\omega_m \omega}{\omega_0^2 - \omega^2}$,^[46,47] $\omega_0 = 2\pi\gamma B_0$ is the precession angular frequency, and $\omega_c = 2\pi \times 3.587 \times 10^9 \text{ rad s}^{-1}$ is the characteristic circular frequency.^[48] B_0 , ω , and ω_m are the magnetic bias field, the angular frequency and the characteristic circular frequency, respectively. According to the Maxwell's equations and the boundary conditions, one may readily calculate the dispersion equations in the above three "arms," and the equations are written as follows

$$\frac{\mu_{2r}}{\mu_{1r}} k + \frac{\alpha_1}{\tanh(\alpha_1 d)} + \frac{\mu_{vr}}{\mu_v} \left[\frac{\mu_2}{\mu_1} k + \frac{\alpha}{\tanh(\alpha d)} \right] = 0 \quad (\text{'A'}) \quad (2)$$

$$-\frac{\mu_{2r}}{\mu_{1r}} k + \frac{\alpha_1}{\tanh(\alpha_1 d)} + \frac{\mu_{vr}}{\mu_v} \left[\frac{\mu_2}{\mu_1} k + \frac{\alpha}{\tanh(\alpha d)} \right] = 0 \quad (\text{'B'}) \quad (3)$$

$$\frac{\mu_{2r}}{\mu_{1r}} k + \frac{\alpha_1}{\tanh(\alpha_1 d)} = 0 \quad (\text{'C'}) \quad (4)$$

where α_1 and α are the attenuation coefficients of the surface magnetoplasmons (SMPs) in the YIG-1/2 and YIG-3. The complete one-way propagation (COWP) bands are characterized by the asymptotic frequencies (AFs), and deriving from Equations (2)–(4), we find that

$$\begin{aligned} \omega_{AF_P1} &= \omega_r \\ \omega_{AF_P2} &= \omega_0 + \omega_m \\ \omega_{AF_N1} &= \frac{2\omega_0 + \omega_m + \omega_r - \sqrt{(2\omega_0 + \omega_m + \omega_r)^2 - 8\omega_0 \omega_r}}{4} \\ \omega_{AF_N2} &= \frac{2\omega_0 + \omega_m + \omega_r + \sqrt{(2\omega_0 + \omega_m + \omega_r)^2 - 8\omega_0 \omega_r}}{4} \end{aligned} \quad (5)$$

for 'A', and

$$\begin{aligned} \omega_{AF_P1} &= \frac{-(2\omega_0 + \omega_m - \omega_r) + \sqrt{(2\omega_0 + \omega_m - \omega_r)^2 + 8\omega_0 \omega_r}}{4} \\ \omega_{AF_P2} &= \omega_0 + \omega_m \\ \omega_{AF_N1} &= \omega_r \\ \omega_{AF_N2} &= \frac{2\omega_0 + \omega_m - \omega_r + \sqrt{(2\omega_0 + \omega_m - \omega_r)^2 + 8\omega_0 \omega_r}}{4} \end{aligned} \quad (6)$$

for 'B', and

$$\omega_{AF_P} = \omega_r \quad (7)$$

for 'C'. We note here that ω_{AF_P} and ω_{AF_N} are the AFs for $k \rightarrow +\infty$ and $k \rightarrow -\infty$, respectively. It is clear that the three arms possess one same AF, that is, $\omega_{AF} = \omega_r$, which is the only AF in the arm 'C' while the other arms have two additional AFs. To further explore the dispersion relations in the arms, we plotted the dispersion diagram for $\omega_0 = 0.5\omega_m$ ($\omega_m = 10\pi \times 10^9 \text{ rad s}^{-1}$, the characteristic circular frequency) and $d = 0.05\lambda_m$ ($\lambda_m = 2\pi c/\omega_m$). In this case, as shown in Figure 2a, there are two COWP regions in the arm 'A', and four AFs (marked by arrows) are observed as well.

Moreover, the waves in both COWP regions can only propagate in the same direction, that is, +x direction. Similarly, two COWP bands are found in the arm 'B' (see Figure 2b) whereas the SMPs in the lower COWP_N band propagate in the opposite direction, that is, in the -x direction. Furthermore, only one COWP_P band is observed in the arm 'C' (see Figure 2c). The COWP bands in the three structures are $0.1482\omega_m < \omega < 0.7174\omega_m$ (COWP_P1) and $1.2105\omega_m < \omega < 1.5\omega_m$ (COWP_P2) for the arm 'A', $0.2105\omega_m < \omega < 0.7174\omega_m$ (COWP_N) and $0.8660\omega_m < \omega < 1.5\omega_m$ (COWP_P) for the arm 'B', and $0 < \omega < 0.7174\omega_m$ (COWP_P) for the arm 'C'. Notably, the lower limit of the COWP_P band in the arm 'B' is not ω_{AF_N2} because it is less than $\omega_s (= \sqrt{\omega_0(\omega_0 + \omega_m)})$ that indicates the edge of the lower bulk zone. Also crucial is the fact that the COWP bands of the SMPs in the three arms overlap with each other in some regions, for example, $0.2105\omega_m < \omega < 0.7174\omega_m$ region. Nevertheless, as shown in Figure 2d, the guiding waves ("P-mode") within the overlapped band in the arm 'A' of the Y-shaped module can not couple to the opposite modes ("N-mode") in the arm 'B' but can propagate to the arm 'C' due to the robust one-way propagation property. Similarly, there is another one-way channel between the arms 'B' and 'C'. As shown in Figure 2e,f, the arm 'B' is equivalent to the arm '-B' in which the EM waves within the overlapped band have positive group velocities. Because of the symmetry, the arm '-A' in this case can only sustain the "N-mode" (see Figure 2e).

In short, the waves in the arms 'A' ('-A') and 'B' ('-B') can only propagate toward the joint of the module while the waves in the output arm 'C' always depart from the joint, constructing two independent one-way channels. Besides, for $1.2105\omega_m < \omega < 1.409\omega_m$, the corresponding guiding waves in the arm 'A' can only travel to the arm 'B' since there are no EM modes in the arm 'C'. The black points in Figure 2 indicate the cut-off frequencies (ω_{CF}) of the SMPs and the bulk modes, which may affect the boundaries of the COWP bands.

In order to further explore the broad COWP band, we studied the correlation between d and ω_{CF} in Figure 3a–c as $\omega_c = 0.5\omega_m$. As a result, the COWP bands in the arms 'A', 'B', and 'C' remain almost the same for thin cases, while for $d > 0.067\lambda_m$, the lower COWP bands in the arms 'A' and 'B' become narrow because of the drop-down bulk modes. Moreover, according to our calculation, we found that $\omega_{CF} > 1.5\omega_m$ as $d < 0.047\lambda_m$. Furthermore, we plot AFs and ω_s as a function of ω_0 as $d = 0.05\lambda_m$ to demonstrate the impact of the EMF on the COWP bands. As demonstrated in Figure 3d, the COWP_P1 gradually narrows down when enlarging B_0 while the COWP_P2 is slightly widened when enhancing the EMF in the arm 'A'. Complicated change of the COWP bands is observed in

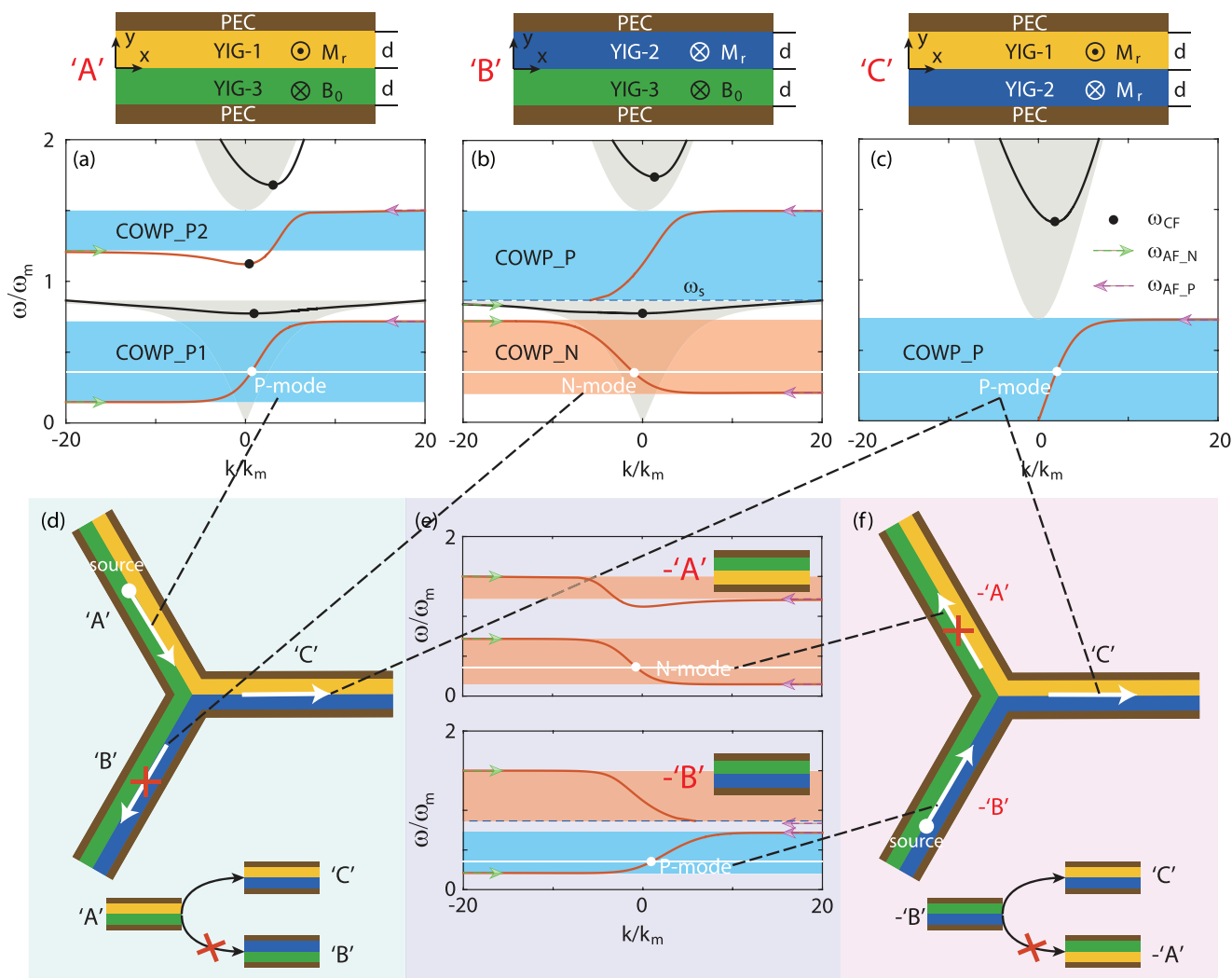


Figure 2. The dispersion diagram of three arms, that is, a) 'A', b) 'B', and c) 'C', of the Y-shaped logical module. The red and black lines indicate the surface modes and lowest-order bulk modes, respectively. The other parameters are $\omega_0 = 0.5\omega_m$, $d = 0.05\lambda_m$, and $\omega_r = 2\pi \times 3.587 \times 10^9$ rad s⁻¹. d, f) Two one-way channels in the Y-shaped module. e) The dispersion diagram of the arms '-A' and '-B'.

Figure 3e, in which the maximal total bandwidth of the COWP bands in the arm 'B' occurs around $\omega = 0.4\omega_m$. Additionally, the one-way region of the arm 'C', different from the arms 'A' and 'B', remains unchanged (see Figure 3f) regardless of the EMF because this arm only contains the YIG with remanence. To achieve the broadband optical logic operation based on unidirectional modes, relatively broad COWP bands are required. Thus, according to the above analyses, we choose $d = 0.04\lambda_m$ and $\omega_r = 0.4\omega_m$ in designing the AODLS in the following work. We note that there are multiple band gaps in the dispersion diagrams of the SMPs, which should have further interesting uses in optical isolators and switches. In this work, however, we just focus on the unidirectional modes and their related applications in the logic gates (LGs) and logic operations.

Similar to Figure 2a,b, **Figure 4a,d** shows the dispersion diagrams of the arms 'A' and 'B' as $d = 0.04\lambda_m$ and $\omega_0 = 0.4\omega_m$, and the bandwidths of the COWP bands in the arms 'A' and 'B' are respectively $0.5906\omega_m$ (COWP_P1, $0.1268\omega_m < \omega < 0.7174\omega_m$), $0.2681\omega_m$ (COWP_P2, $1.1319\omega_m < \omega < 1.4\omega_m$), $0.5225\omega_m$ (COWP_N,

$0.1949\omega_m < \omega < 0.7174\omega_m$), and $0.6638\omega_m$ (COWP_P, $0.7362\omega_m < \omega < 1.4\omega_m$). Moreover, we further calculated the corresponding group velocities (v_g) of the unidirectional modes in Figure 4b,e. As one can see, the EM signals in the COWP bands could propagate with $v_g > 0.05c$ (c is the light speed in vacuum). We note here that, due to the absence of the delay time and fan-in/fan-out,^[49] the information processing in the proposed device should be faster than in the electrical devices. In addition, the loss effect on the arms was also studied as the damping coefficient $\nu = 10^{-3}\omega$ as seen in Figure 4c,f. One can easily see the difference between the propagation lengths (L) in the upper and the lower COWP bands. More specifically, the EM waves in the COWP_P1 band in the arm 'A' could propagate about ten times longer than in the COWP_P2 band. Hence, the lower COWP band should be more suitable for the logic operations. According to our calculation, the unidirectional EM waves in the arm 'C' can always propagate with low loss ($L \geq 10^3$ mm). By far, we have studied the propagation characteristics, including the unidirectionality and low loss, in three arms of the basic Y-shaped module of the AODLS. In what

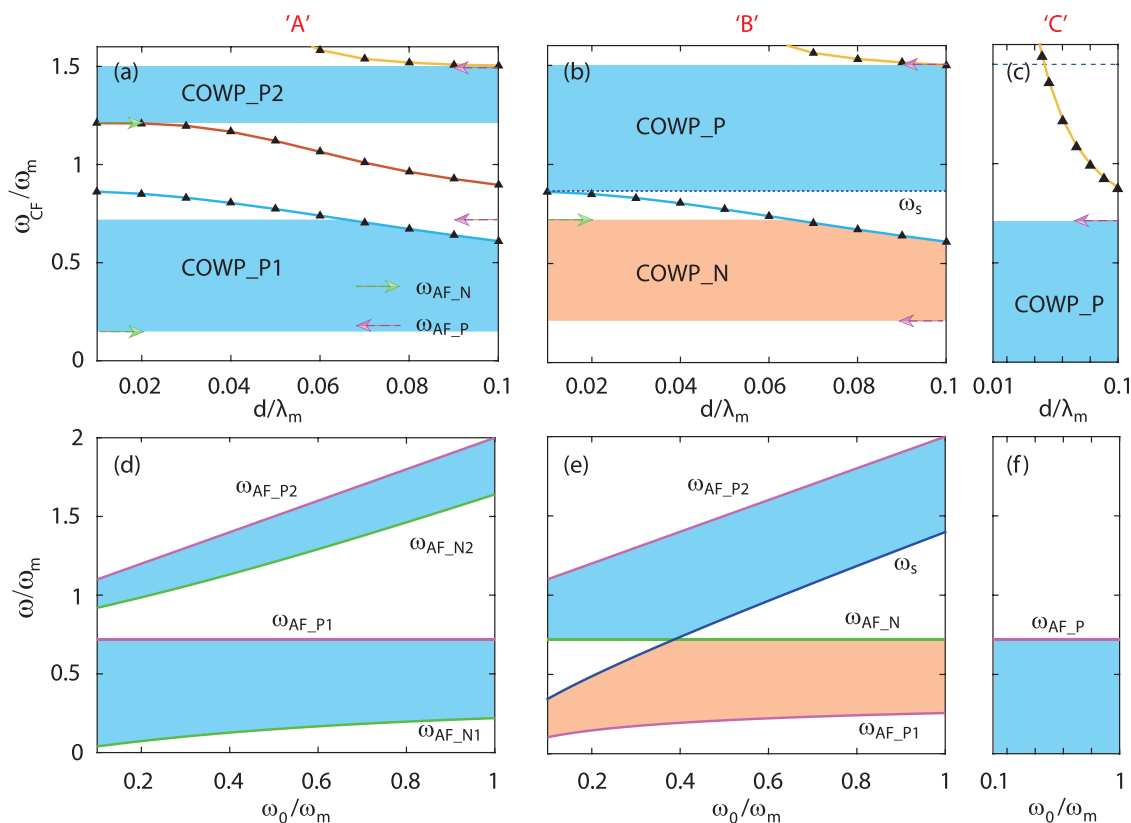


Figure 3. The cut-off frequencies (marked by black points in Figure 2) as a function of the thickness parameter in the arms a) 'A', b) 'B', and c) 'C'. d–f) The limits of the COWP bands as a function of ω_0 in the arms 'A', 'B', and 'C'.

follows, we will show how the one-way channels or the Y-shaped module can work as the LGs.

3. Realization of the Basic Logic Gates

As we discussed above in the proposed Y-shaped structure in Figure 4, the arms 'A' and 'C' can support unidirectionally forward propagating modes whereas the arm 'B' can only support backward modes. Here we consider the operating frequency within the region of $0.1949\omega_m < \omega < 0.7174\omega_m$ (see Figure 4). In this condition, the launched one-way waves in arm 'A', due to the unidirectionality, could near-perfectly couple with the forward modes in arm 'C' and output in the end. Similar unidirectional signal transmission happens in the 'B'–'C' channel. Due to the two one-way channels, our proposed Y-shaped module can work as the OR and AND gate.

On the one hand, for the OR gate, we treat the existence of the EM signal in the arms as logic "1" while, on the contrary, the zero-energy state is regarded as logic "0" (see Figure 5b). The default value/state in the OR gate is set to be logic "0". Relying on such a principle, any one of the input logic "1" (input unidirectional EM signal) will lead to the output logic "1" (output unidirectional EM signal), indicating the OR operation. On the other hand, the AND operation requires two input logic "1" to generate output logic "1". Nevertheless, the positive logic used in the OR gate can not be used to achieve the AND gate. Here, we introduce the negative logic to achieve the AND gate

based on the Y-shaped module. As contrasted with the OR gate, in the AND gate, we treat the EM propagation as logic "0" and treat no energy flow as logic "1," and set the default value to be logic "1" for both inputs and output (see Figure 5c). In the AND gate, any one of the input EM waves (logic "0") will lead to output logic "0".

By utilizing the similar negative logic, the Y-shaped module can also serve as the NOT gate. As shown in Figure 5d, three channels of the proposed module can all work as the NOT gate, in which the EM energy represents logic "1" for the input arm and logic "0" (negative logic) for the output (see Figure 5e). The input and output default values are logic "0" and logic "1," respectively. In this condition, the launched EM waves unidirectionally travel through the 'A'–'C', ...'B'–'C', or 'A'–'B' channels, and meanwhile the input logic "1" turns to output logic "0," indicating the NOT operation. The colored panels in Figure 5a,e demonstrate the operating bands of the inputs of the LGs. It is worth noting that in what follows, all the parameters of the Y-shaped module are the same as those in Figure 4.

Different from the other optical LGs,^[8,11,12] our designed MO module can achieve multiple LGs functionalities in the same device without modifying. For instance, in Figure 6, we performed two simulations in the Y-shaped module as $f = 0.5f_m$ by using the finite element method (FEM). In the first simulation (leftmost picture), the EM wave was excited in arm 'A' and as we expected, it traveled through the joint part and unidirectionally coupled into arm 'C'. In the next simulation, the EM wave with

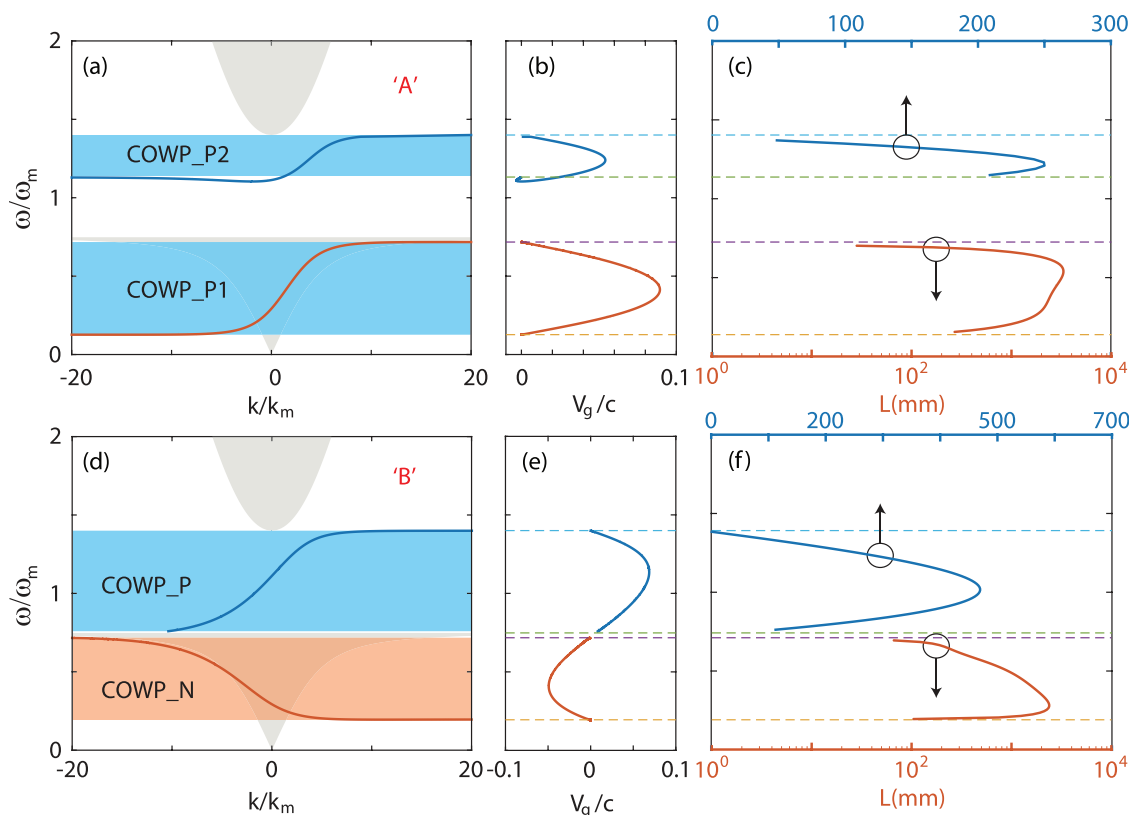


Figure 4. The dispersion diagrams of a) the 'A' and d) the 'B' configurations as $d = 0.04\lambda_m$ and $\omega_0 = 0.4\omega_m$. b,e) The group velocities and c,f) the propagation distances of the one-way modes in the COWP regions. In the lossy cases, the relaxation angular frequency $\nu = 10^{-3}\omega$.

a backward propagation direction was launched in the arm 'B' and similarly, it propagated along the 'B'-'C' channel without backscattering. Accordingly, the input logic states in the first simulation are respectively ["1", "0"] for the OR gate, ["0", "1"] for the AND gate and ["1",] for the NOT gate. On the contrary, the input logic states in the second simulation are respectively ["0", "1"] for the OR gate, ["1", "0"] for the AND gate, and [, "1"] for the NOT gate. Based on the proposed theory in Figure 5, the output logic states in the two simulations are the same for both logic operations. The more clear results are exhibited in the rightmost truth tables. Due to the negative logic, the output logic states of the simulations are logic "0" in the AND and NOT operations while in the OR operation, the output read logic "1". Consequently, the Y-shaped module is capable of being used in multiple logic operations, and it is a multi-function LGs, which is potential for high-performance optical communication or calculation.

In addition, the Y-shaped module can also serve as the universal gates, that is, the NOR and NAND gates. For the NOR operation, the principle is similar to that of the NOT gate except for the number of input signals. As shown in Figure 7a, because of the one-way characteristic, either input with logic "1" (EM signal) will lead to the output logic "0," implying the NOR operation. Moreover, the NAND gate can be achieved by thoroughly utilizing the negative logic in the NOR gate. In a word, completely replacing the logic states in the NOR gate to the opposite

ones, that is, "1" \rightarrow "0" and "0" \rightarrow "1" (see Figure 7b,c). We further performed another two similar simulations like the ones in Figure 6 to verify the NOR and NAND operations for a different working frequency $f = 0.4f_m$. As demonstrated in Figure 7d,e, the different inputs logic states will lead to output logic "0" for the NOR gate and logic "1" for the NAND gate. All the results of the simulations fit well with our theoretical analyses. Thus, we conclude here that our proposed Y-shaped module can not only work as the single basic LG, that is, the OR, AND, NOT, NOR, and NAND gates, but it can also work as a multiple outputs logical device. Besides, the XOR and XNOR gates could be easily achieved by comparing the EM energy intensity of the output and inputs of the Y-shaped configuration. For example, we could treat the existence of the output EM signal as logic "1" only if there is only one input EM signal, implying the XOR operation. One should also note that the logic states in our proposed LGs directly rely on the existence of the robust unidirectional EM signal, which is far more precise than the other proposed LGs. For example, in the simulation of OR operation (see Figure 6), the intensity of the logic "0" is nearly zero ($P_0 \approx 0$) while the intensity of the logic "1" is obvious nonzero ($P_1 \neq 0$), implying infinite CR and ER,^[6] and the Er in this case is negligible since it is easy to distinguish two logic states. Our designed LGs based on the one-way channels/modes can work in continuous and relatively broad COWP bands, which is another distinct feature of this kind of all-optical LGs.

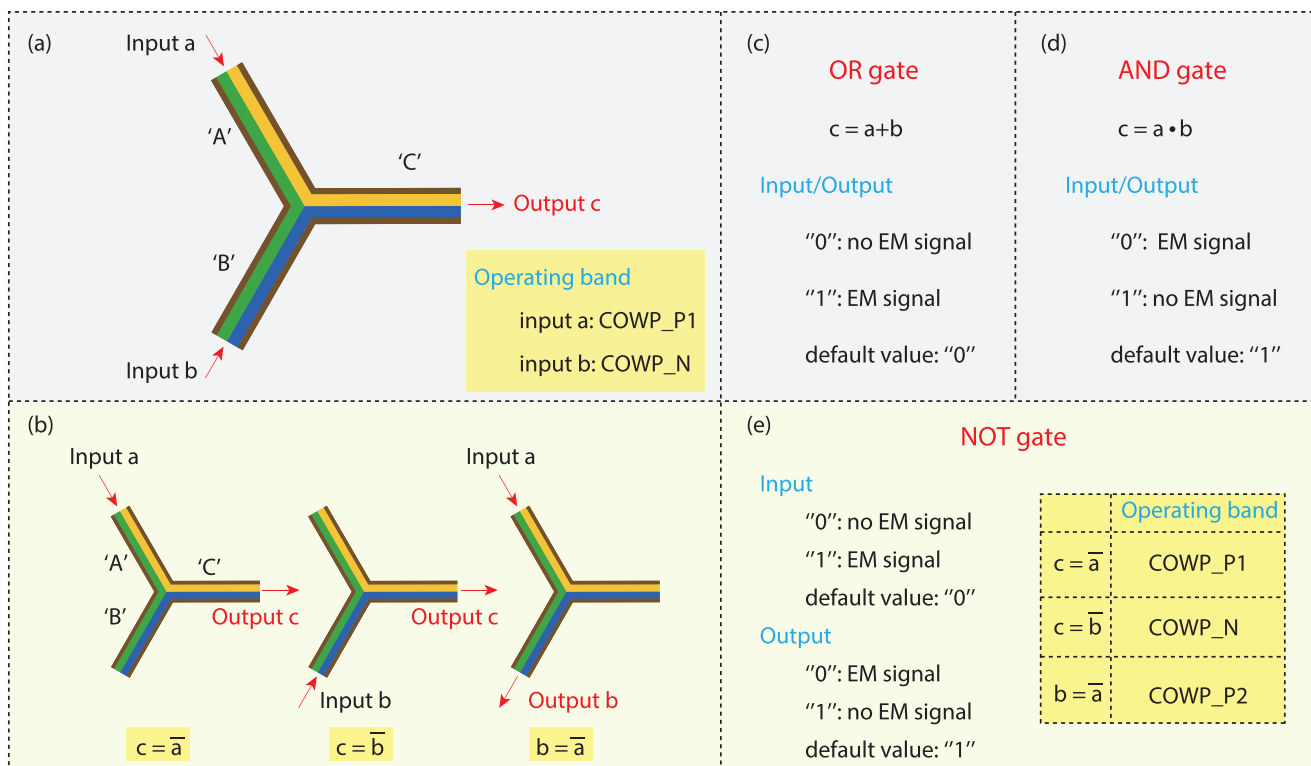


Figure 5. Basic OR, AND, and NOT gates based on the Y-shaped module. a) The schematic diagram of the OR and AND gates with two inputs and one output. b) The schematic diagram of the NOT gates with one input and one output. c–e) The theory of realization of the OR, AND, and NOT digital LGs.

4. The AODLS for Multi-Input and/or Multi-Output Logic Operations

Optical computations are characterized by super-fast data transmission relying on fan-in and fan-out,^[49] and our proposed unidirectional-modes-based LGs indeed have a continuous, broad operating band. Moreover, since the basic LGs have been achieved, by utilizing the Y-shaped module consisting of three

YIG-based arms, in what follows, we will show how such a module could be used in designing AODLS with the ability to expand to multi-input and/or -output optical logic system. The schematic of the AODLS is shown on the left side of **Figure 8**. It needs to be emphasized that, in this subsection, we only consider the logic operations in the lower COWP regions, that is, $0.1948\omega_m < \omega < 0.7174\omega_m$. To clearly show the possible signal

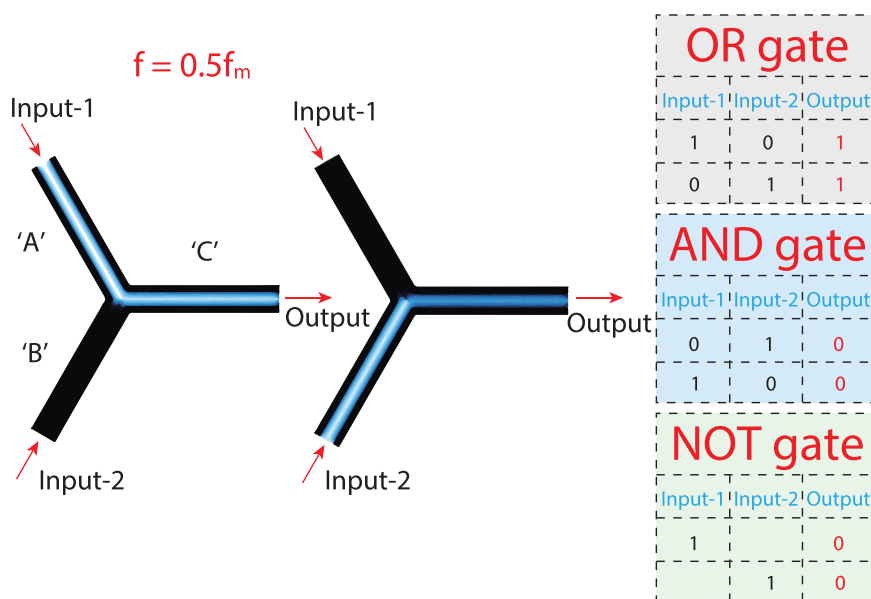


Figure 6. Numerical simulations and the truth tables of the achievement of the OR, AND, and NOT gates in one shot.

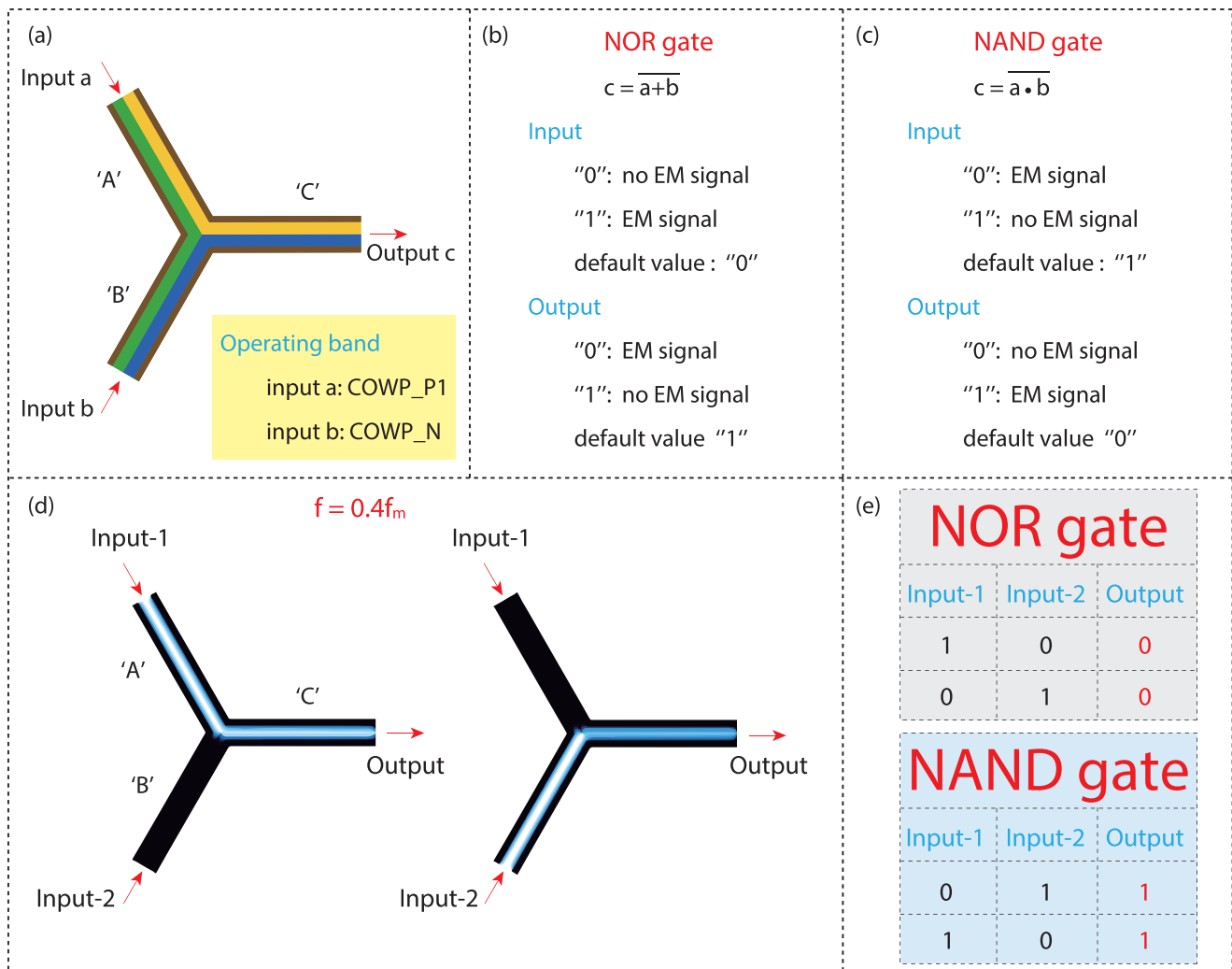


Figure 7. a) The schematic diagram of the NOR and NAND gates. b,c) The theory of realization of the NOR and NAND gates. d,e) Numerical simulations and the truth tables of the NOR and NAND gates.

transmission, we added the black arrows in the schematic of the AODLS, which represent the propagation directions of the one-way channels. In the AODLS, six alternative outputs or logic operations can be chosen for two inputs. It is worth mentioning that the AODLS works with two inputs can be easily extended to the four-input logic device by suitably assembling the Y-shaped modules. Besides, the impinge part/module, as shown in the enlarged upper right picture in Figure 8, is a left-hand connected 'A–B–C' module while the above Y-shaped module has a right-hand connection. In this incident module, the input EM waves from the arm 'C' can simultaneously transmit to the arms 'A' and 'B'. More clear results are displayed in the right diagrams, in which we injected an input EM signal with $f = 0.5f_m$, and three air holes with radius $r = 1$ mm were put on the YIG–YIG interfaces to further verify the robust unidirectionality of the incident EM modes. As one can see, the input EM wave perfectly bypassed the air hole in the arm 'C' and then split into two EM waves which still possess the robust one-way propagation characteristic. Thus, the incident module guarantees the NOT logic operation while part of the EM signal participates in other logic operations.

In **Figure 9**, we performed a FEM simulation in our designed AODLS. As expected, the input signal was unidirectionally transmitted along the one-way channels and exited via the outputs. Virtually no crosstalk or noise was observed during the logic operations, and the propagation characteristics of the EM wave are perfectly consistent with our theoretical analyses. More importantly, the proposed AODLS exhibits exotic multi-output logic operation with one-time input based on the robust unidirectional propagation of the EM signal(s). The OR, AND, NOT, NOR, and NAND gates were simultaneously achieved as demonstrated in the shaded truth tables in Figure 9. Moreover, the AODLS has great potential for complex logic operations due to its expansibility, precision, and broadband characteristic. Theoretically, no matter how complex the logic operation is, one can always achieve the specific logic operation by combining the unidirectional EM signal (logic "1" or "0") and the input–output intensities/phases. Furthermore, the unidirectional modes-based LGs, compared to the electrical ones, are more efficient since it is far easier to distinguish the existence of the EM signal(s) than to differentiate the relatively high and low levels.

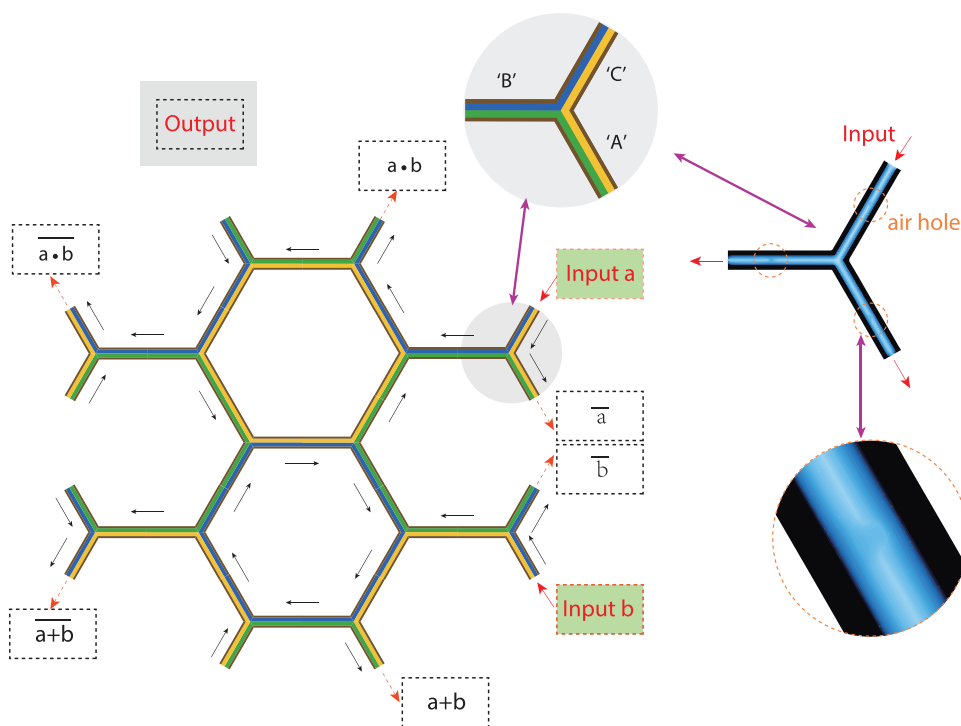


Figure 8. Realization of multiport parallel logical computation system based on the Y-shaped module. The black arrows represent the path directions for the EM waves/signals.

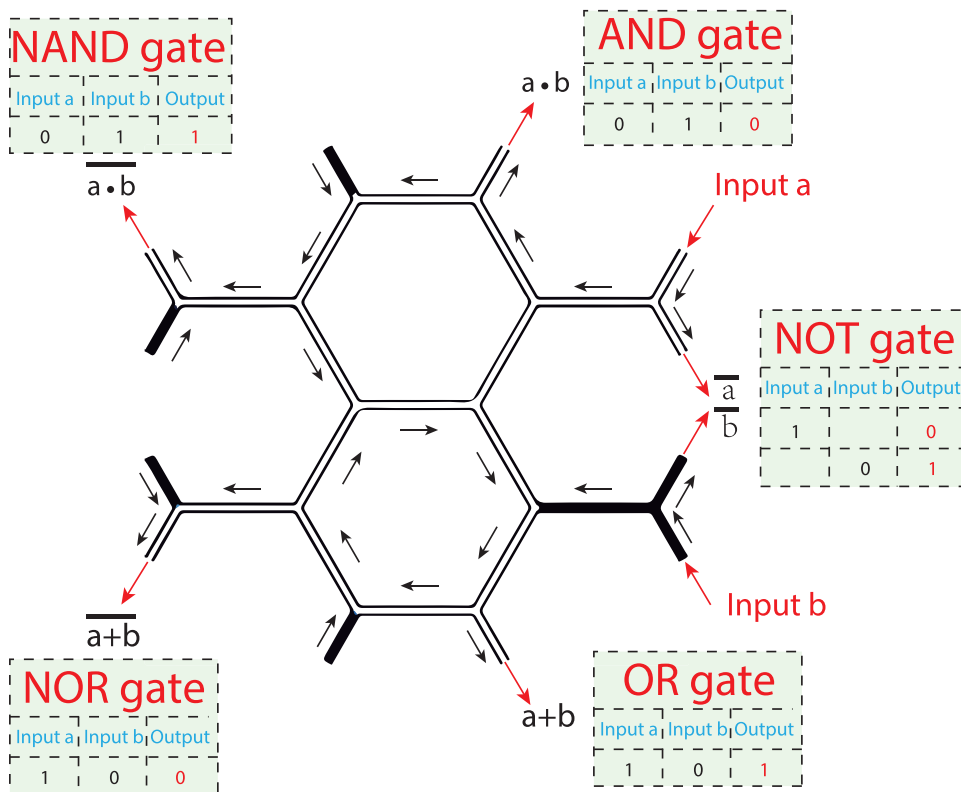


Figure 9. Multi-output logic operation in the AODLS as the input EM wave with $f = 0.5f_m$.

5. Conclusion

In summary, we have proposed a novel, robust, AODLS based on unidirectional modes. In the theoretical analysis, oppositely propagating SMPs are identified in the Y-shaped module. Relying on broadband one-way channels and/or the negative logic concept, we have shown that the Y-shaped module can be used to achieve all basic logic gates independently or simultaneously. Moreover, we have further designed the AODLS based on the Y-shaped configurations. By simply jointing the modules, we have achieved multi-output logic operations, which imply parallel computation. All logic operations are dependent on the existence of unidirectional EM signals, resulting in ultra-precise all-optical logic operations. We emphasize that the proposed microwave AODLS could be extended to higher frequency regimes once opposite (one-way) SMPs are found and judiciously utilized.^[50] Owing to the broad operating band, robust signal transmission, precision, composability, and extensibility, our proposed AODLS could become a novel platform for optical calculations and optical communication, and it is here believed that it has a great potential for designing integrated optical circuits.

Acknowledgements

J.X. and Y.L. acknowledge the support of the Science and Technology Strategic Cooperation Programs of Luzhou Municipal People's Government and Southwest Medical University (2019LZXNYD)18). J.X. thanks the financial support from Funding of Southwest Medical University (20/00160222). F.K. financially thanks for the support of the European Union's Horizon 2020 research and innovation program (H2020, no. 609405) under the Marie Skłodowska-Curie grant agreement no. 713683 (COFUNDfellowsDTU), the "Spring Buds Talent" Program and its starting grant from Ningbo Institute of Materials Technology and Engineering (NIMTE) Chinese Academy of Sciences (CAS), and the "Double Hundred Talent" project and the starting grant from Sichuan University. K.L.T. was supported by the General Secretariat for Research and Technology (GSRT) and the Hellenic Foundation for Research and Innovation (HFRI) under Grant No. 4509.

Conflict of Interest

The authors declare no conflict of interest.

Data Availability Statement

The data that support the findings of this study are available from the corresponding author upon reasonable request.

Keywords

logic gates, magneto-optical systems, unidirectional modes

Received: August 4, 2022

Revised: September 6, 2022

Published online: November 14, 2022

- [1] I. L. Markov, *Nature* **2014**, 512, 147.
- [2] H. Yang, V. Khayrudinov, V. Dhaka, H. Jiang, A. Autere, H. Lipsanen, Z. Sun, H. Jussila, *Sci. Adv.* **2018**, 4, eaar7954.
- [3] J. Hardy, J. Shamir, *Opt. Express* **2007**, 15, 150.
- [4] Q. Xu, M. Lipson, *Opt. Express* **2007**, 15, 924.
- [5] A. Fushimi, T. Tanabe, *Opt. Express* **2014**, 22, 4466.
- [6] J. K. Rakshit, J. N. Roy, *Opt. Commun.* **2014**, 321, 38.
- [7] C. Qiu, W. Gao, R. Soref, J. T. Robinson, Q. Xu, *Opt. Lett.* **2014**, 39, 6767.
- [8] Y. Zhang, Y. Lu, M. Yuan, Y. Xu, Q. Xu, Q. Yang, Y. Liu, J. Gu, Y. Li, Z. Tian, C. Ouyang, W. Zhang, J. Han, *Adv. Opt. Mater.* **2022**, 10, 2102561.
- [9] C. Taraphdar, T. Chattopadhyay, J. N. Roy, *Opt. Laser Technol.* **2010**, 42, 249.
- [10] A. Kotb, K. E. Zoiros, C. Guo, *Opt. Laser Technol.* **2018**, 108, 426.
- [11] X. Yang, X. Hu, H. Yang, Q. Gong, *Nanophotonics* **2017**, 6, 365.
- [12] Y. Fu, X. Hu, C. Lu, S. Yue, H. Yang, Q. Gong, *Nano Lett.* **2012**, 12, 5784.
- [13] Y. Sang, X. Wu, S. S. Raja, C.-Y. Wang, H. Li, Y. Ding, D. Liu, J. Zhou, H. Ahn, S. Gwo, J. Shi, *Adv. Opt. Mater.* **2018**, 6, 1701368.
- [14] H. Wei, Z. Li, X. Tian, Z. Wang, F. Cong, N. Liu, S. Zhang, P. Nordlander, N. J. Halas, H. Xu, *Nano Lett.* **2011**, 11, 471.
- [15] Y. Liu, F. Qin, Z.-M. Meng, F. Zhou, Q.-H. Mao, Z.-Y. Li, *Opt. Express* **2011**, 19, 1945.
- [16] A. Coelho, M. Costa, A. Ferreira, M. Da Silva, M. Lyra, A. Sombra, *J. Lightwave Technol.* **2012**, 31, 731.
- [17] Y. Fu, X. Hu, Q. Gong, *Phys. Lett. A* **2013**, 377, 329.
- [18] Y. Wang, W. Liu, Z. Ji, G. Modi, M. Hwang, R. Agarwal, *Nano Lett.* **2020**, 20, 8796.
- [19] T. Paraiso, M. Wouters, Y. Léger, F. Morier-Genoud, B. Deveaud-Plédran, *Nat. Mater.* **2010**, 9, 655.
- [20] A. Takeuchi, H. Yamagishi, O. Oki, M. Morimoto, M. Irie, Y. Yamamoto, *Adv. Funct. Mater.* **2021**, 31, 2103685.
- [21] J. Ding, M. Kostylev, A. Adeyeye, *Appl. Phys. Lett.* **2012**, 100, 073114.
- [22] W. Yu, J. Lan, J. Xiao, *Phys. Rev. Appl.* **2020**, 13, 024055.
- [23] R. Sordan, F. Traversi, V. Russo, *Appl. Phys. Lett.* **2009**, 94, 51.
- [24] S.-L. Li, H. Miyazaki, A. Kumatani, A. Kanda, K. Tsukagoshi, *Nano Lett.* **2010**, 10, 2357.
- [25] Y. T. Lee, J.-H. Kang, K. Kwak, J. Ahn, H. T. Choi, B.-K. Ju, S. H. Shokouh, S. Im, M.-C. Park, D. K. Hwang, *ACS Photonics* **2018**, 5, 4745.
- [26] Q. Ma, G. Ren, K. Xu, J. Z. Ou, *Adv. Opt. Mater.* **2021**, 9, 2001313.
- [27] H. Wei, Z. Wang, X. Tian, M. Käll, H. Xu, *Nat. Commun.* **2011**, 2, 387.
- [28] V. R. Almeida, C. A. Barrios, R. R. Panepucci, M. Lipson, *Nature* **2004**, 431, 1081.
- [29] Y. Chen, Y. Cheng, R. Zhu, F. Wang, H. Cheng, Z. Liu, C. Fan, Y. Xue, Z. Yu, J. Zhu, X. Hu, Q. Gong, *Sci. China: Phys., Mech. Astron.* **2019**, 62, 44201.
- [30] J. Xu, S. Xiao, C. Wu, H. Zhang, X. Deng, L. Shen, *Opt. Express* **2019**, 27, 10659.
- [31] K. L. Tsakmakidis, L. Shen, S. A. Schulz, X. Zheng, J. Upham, X. Deng, H. Altug, A. F. Vakakis, R. W. Boyd, *Science* **2017**, 356, 1260.
- [32] J. Xu, S. Xiao, P. He, Y. Wang, Y. Shen, L. Hong, Y. Luo, B. He, *Opt. Express* **2022**, 30, 3941.
- [33] S. A. H. Gangaraj, B. Jin, C. Argyropoulos, F. Monticone, *Phys. Rev. Appl.* **2020**, 14, 054061.
- [34] F. Monticone, *Nat. Photonics* **2020**, 14, 461.
- [35] M. Kim, W. Gao, D. Lee, T. Ha, T.-T. Kim, S. Zhang, J. Rho, *Adv. Opt. Mater.* **2019**, 7, 1900900.
- [36] L. Lu, J. D. Joannopoulos, M. Soljačić, *Nat. Photonics* **2014**, 8, 821.
- [37] M. Wang, R.-Y. Zhang, L. Zhang, D. Wang, Q. Guo, Z.-Q. Zhang, C. T. Chan, *Phys. Rev. Lett.* **2021**, 126, 067401.

- [38] Z. Wang, Y. Chong, J. D. Joannopoulos, M. Soljačić, *Nature* **2009**, 461, 772.
- [39] K. L. Tsakmakidis, C. Hermann, A. Klaedtke, C. Jamois, O. Hess, *Phys. Rev. B* **2006**, 73, 085104.
- [40] J. Xu, Q. Shen, K. Yuan, X. Deng, Y. Shen, H. Zhang, C. Wu, S. Xiao, L. Shen, *Opt. Commun.* **2020**, 473, 125999.
- [41] K. L. Tsakmakidis, K. Baskourellos, T. Stefański, *Appl. Phys. Lett.* **2021**, 119, 190501.
- [42] L. Shen, J. Xu, Y. You, K. Yuan, X. Deng, *IEEE Photonics Technol. Lett.* **2017**, 30, 133.
- [43] Z. Wang, Y. Chong, J. D. Joannopoulos, M. Soljačić, *Phys. Rev. Lett.* **2008**, 100, 013905.
- [44] L. Bi, J. Hu, P. Jiang, D. H. Kim, G. F. Dionne, L. C. Kimerling, C. Ross, *Nat. Photonics* **2011**, 5, 758.
- [45] J. Shamir, *Opt. Commun.* **2013**, 291, 133.
- [46] L. Hong, Y. Wang, Y. Shen, X. Deng, K. Yuan, S. Xiao, J. Xu, *Opt. Mater. Express* **2021**, 11, 2975.
- [47] J. Xu, X. Deng, H. Zhang, C. Wu, M. Wubs, S. Xiao, L. Shen, *J. Opt.* **2020**, 22, 025003.
- [48] D. M. Pozar, *Microwave Engineering*, John Wiley & Sons, New York **2011**.
- [49] H. J. Caulfield, S. Dolev, *Nat. Photonics* **2010**, 4, 261.
- [50] B. Bahari, A. Ndao, F. Vallini, A. El Amili, Y. Fainman, B. Kanté, *Science* **2017**, 358, 636.